International Forum on Aeroelasticity and Structural Dynamics
IFASD 2017
25-28 June 2017 Como, Italy

ASSESSMENT OF ADVANCED FLUTTER FLIGHT TEST TECHNIQUES AND FLUTTER BOUNDARY PREDICTION METHODS

Maj. Michael Iovnovich and Lt. Tzlil Nahom[1], Lt. Michael Presman and Lt. Dorin Avsaid and Maj. Tomer Braier[2], Daniella E. Raveh[3]

[1]Flight Sciences Branch
Israeli Air Force
Tel-Aviv, Israel
smichael.iov@gmail.com

[2]Flight Test Center
Israeli Air Force
Tel-Nof Airbase, Israel

[3]Faculty of Aerospace Engineering
Technion - IIT
Haifa 32000, Israel
daniella@technion.ac.il

Keywords: Experimental methods, Flutter flight testing, ARMA, Operational modal analysis

Abstract: The paper presents an experimental study, conducted at the Israeli Air Force, aimed at the assessment of several advanced flutter flight test techniques that are designed to improve the efficiency and accuracy of flutter tests. These include the auto-regresive moving-avarage (ARMA) and operational modal analysis (OMA) system identification methods, the use of various system stability parameters, and the use of atmospheric turbulence versus prescribed flaperon motion as the source of structural response excitation. The methods were evaluated based on data from a dedicated transonic flight test of the F-16 platform. All of the tested methods were able to accurately predict the instability onset. The OMA method has the advantage that it does not require a priori knowledge of the instability mechanism (participating modes and approximate flutter frequency). However, it requires delicate identification of the participating modes, thus making it less suitable for real time processing. The ARMA method, on the other hand, is easier to implement, and straight forward to use in real time. Both methods require relatively large data records, of about 60 seconds at each test point. Excitation by atmospheric turbulence was found to be adequate in the current test case, in which the modes are lightly damped, and highly suitable for system identification methods that rely on stochastic inputs. While further assessment is required for cases of highly damped modes and of flight in low turbulence levels, the use of ARMA and OMA methods based on responses to atmospheric turbulence appears to offer an accurate and cost effective flutter testing methodology.

1 INTRODUCTION

Aeroelastic flutter is a destructive instability phenomenon for which dedicated flight test campaigns are considered compulsory by the airworthiness regulations. In these tests, the dynamic

characteristics of the aeroelastic system are interpreted from measurements of aircraft structural responses to external excitations. Over the years, several Advanced Flutter Flight Test Techniques (AFFTTs) were developed in order to improve the efficiency and accuracy of flutter flight tests, by using various excitation techniques, system identification and estimation methods, system stability parameters and flutter boundary prediction methods [1–9].

From the point of view of excitation techniques, most methods may be adjusted to a single frequency harmonic external excitation of each suspected aeroelastic mode, broadband frequency sweep, or random excitation of the full spectra of interest. These types of excitation may be applied to the structure using the aircraft's control surfaces or by means of dedicated actuation equipment. While for the single frequency excitation case the system dynamic characteristics may be extracted manually using the log-dec formula [10], broadband excitations require specific signal processing and curve-fitting procedures [2] or the use of system identification techniques [3–5, 7] to identify the stability parameters. Some of the latter methods may also be used in case of natural structural excitation by air turbulence, assuming the probabilistic nature of the excitation.

The most basic method for flutter flight tests is the Modal Damping Extrapolation (MDE) method [10]. According to this method, modal dampings are used directly as the system stability parameters. The major drawback of this approach is that the variation of modal dampings with flow conditions is generally a priori unknown. In practice, considerable decrease in flutter-suspected modal dampings may sometimes be observable only near the flutter onset. This reduces the efficiency of the MDE method, making it practically unsuitable for reliable flutter boundary prediction based on subcritical test points data. As an alternative, the Flutter Margin (FM) method [1] employs the Routh-Hurwitz stability criterion [11] to identify a more robust stability parameter. According to this method, the aeroelastic system characteristic equation values are evaluated at each test point based on the modal parameters of the coupled modes. These values are identified as the FM stability parameter. As the system approaches instability, the FM stability parameter approaches zero as a quadratic function of the dynamic pressure, thus the flutter envelope may be predicted. If the modal parameters extraction is performed in the z complex frequency domain, the Jury stability criterion [12] may be used instead of the Routh-Hurwitz criterion. Using this criterion, a favorable feature of linear variation of the stability parameter with the dynamic pressure may be achieved [13].

The Autoregressive Moving-Average (ARMA) method, originally suggested by Matsuzaki and Ando [3], offers a favorable stability parameter that is extracted using advanced system identification methods from structural responses to atmospheric turbulent excitations, without resorting to external excitation. This discrete-time method assumes the probabilistic distribution and frequency content of the excitation to be normally-distributed random white-noise, thus arguably suitable to describe natural air turbulence excitation. Once the aeroelastic system is identified using system identification techniques, the stability parameter is identified according to the Jury criterion. The ARMA method was originally developed for stationary measurements of a two-mode aeroelastic system. Later publications suggested extended versions of the method for nonstationary measurements [14] and multiple-mode systems [15], featuring advanced versions of the flutter stability parameter [13].

Another novel family of system identification methods for flutter testing are the Operational Modal Analysis (OMA) tools [5, 16–19]. Originally developed from ground vibration test estimation techniques, OMA methods also assume random white-noise external excitation of

the structure, and estimate the non-parametric cross-spectra functions between structural responses at different measurement locations. These spectra functions are then used to identify a parametric Multiple-Input-Multiple-Output (MIMO) model using frequency domain estimation techniques such as Maximum Likelihood (ML) [20], least square (LS) [19], or combined ML–LS [21] approaches. These methods may be used as the basis for the FM stability parameter identification [22].

Evaluation of the AFFTTs mentioned above was carried out by Dimitriadis and Cooper [23,24], as well as by Lind [25] and by Zeng and Kukreja [22]. In the first study, the authors used two test cases, namely a three-degrees-of-freedom, rectangular wing with control surfaces model, and a civil transport aircraft model. The structural responses of these models to external excitations were simulated numerically. These responses were then contaminated with white noise and analyzed according to the different methods. In [25] and [22], a test wing model was assembled to the F-15 fighter aircraft centerline station and flight-tested in the F-15 subsonic flight envelope. The test wing was integrated with measurement sensors and excitation actuators, and tested at 21 points across the envelope before experiencing a destructive flutter incident. The results of these studies emphasize different characteristics and disadvantages of the tested methods. However, applicability to realistic flutter flight testing of complex structures at various flight flow regimes, still requires further evaluation.

The current paper presents assessment and validation of several AFFTT elements, namely the autoregressive moving-average and the operational modal analysis system identification methods, the free air turbulence and forced random excitation techniques, and finally the Jury criterion based and Flutter Margin stability parameters. The methods are evaluated based on dedicated transonic flutter flight tests of the F-16 platform conducted at the Israel Air Force (IAF) Flight Test Center (FTC).

2 THEORETICAL MODEL

Considering a viscously damped, linear, dynamic system of N degrees of freedom (DOF), the system oscillatory motion in the continuous time-domain is given by:

$$Y(t) = \sum_{n=1}^{N} [\hat{A}_n e^{s_n t} + \hat{B}_n e^{\overline{s}_n t}] \tag{1}$$

$$s_n = (-\zeta_n + i\sqrt{1-\zeta_n^2})\omega_n \tag{2}$$

where s is the complex laplace parameter, $\overline{s}$ is the complex conjugate of s, $\hat{A}_n, \hat{B}_n$ are constants and ζ_n, ω_n are the system n-th modal damping ratio and frequency parameters, respectively. For $\zeta_n^2 \ll 1$, the system modal parameters can be extracted directly from s_n by:

$$s_n \cong (-\zeta_n + i)\omega_n \tag{3}$$

$$\omega_n = Im(s_n); \qquad \zeta_n = -\frac{Re(s_n)}{Im(s_n)} \tag{4}$$

Assuming that the system response $Y(t)$ is sampled at a constant interval Δt, $y_i = Y(i\Delta t)$ is the response time series value at sample i with $i = 1..K$. The z complex frequency domain

is commonly known as the discrete equivalent of the laplace domain. The z-transform [12] is defined by:

$$\tilde{Y}(z) = \sum_{n=0}^{\infty} y_n z^{-n} \qquad z = e^{s\Delta t} \tag{5}$$

Substituting equation 3 into 5, we obtain the z-plane roots as functions of the modal parameters:

$$z_n = e^{s_n \Delta t} = e^{-\omega_n \zeta_n \Delta t}[\cos(\omega_n \Delta t) + i \sin(\omega_n \Delta t)] \tag{6}$$
$$|z_n| = e^{-\omega_n \zeta_n \Delta t} \qquad \angle z_n = \omega_n \Delta t$$

Consequently, the modal parameters may be expressed as a function of the z-plane roots by:

$$\omega_n = \frac{|\ln z_n|}{\Delta t} \qquad \zeta_n = -\frac{\ln |z_n|}{|\ln z_n|} \tag{7}$$

2.1 ARMA Model

Assuming any random external excitation to the structure, the ARMA(p,q) model of the aeroelastic system is given by:

$$y_i + \phi_1 y_{i-1} + \phi_2 y_{i-2} + \ldots + \phi_p y_{i-p} = \epsilon_i + \theta_1 \epsilon_{i-1} + \theta_2 \epsilon_{i-2} + \ldots + \theta_q \epsilon_{i-q} \tag{8}$$

where p,q and ϕ_i, θ_i are the Autoregressive (AR) and Moving-average (MA) model orders and constants, respectively. ϵ_i is a time series that represents the normally distributed, white-noise, random sequence with zero mean and an unknown variance of σ^2. In summation notation, equation 8 may be rewritten as:

$$\sum_{n=0}^{p} \phi_n y_{i-n} = \sum_{m=0}^{q} \theta_m \epsilon_{i-m} \tag{9}$$
$$\theta_0 = \phi_0 = 1$$

The AR model order p is directly associated with the system order in the laplace domain, thus for a system with N DOF, the AR order is taken as $p = 2N$. The MA order q is typically taken as $q = p - 1$, however a more general approach to optimize q for best model fitting is by minimization of the Akaike's Information Criterion (AIC) parameter, as described in [3, 26].

Applying the z-transform to equation 9, we obtain:

$$\sum_{n=0}^{p} \phi_n z^{-n} \sum_{n=0}^{\infty} y_n z^{-n} = \sum_{m=0}^{q} \theta_m z^{-m} \sum_{m=0}^{\infty} \epsilon_m z^{-m} \tag{10}$$

using equations 10 and 5, the system transfer function may be identified in the z-plane as:

$$\tilde{H}(z) = \frac{\tilde{Y}(z)}{\tilde{\Upsilon}(z)} = \frac{\sum_{m=0}^{q} \theta_m z^{-m}}{\sum_{n=0}^{p} \phi_n z^{-n}} \tag{11}$$

from which the system characteristic equation may be identified as:

$$G(z) = z^p \sum_{n=0}^{p} \phi_n z^{-n} = z^p + \phi_1 z^{p-1} + \phi_2 z^{p-2} + \ldots + \phi_p \tag{12}$$

$$G(z) = A_p z^p + A_{p-1} z^{p-1} + A_{p-2} z^{p-2} + \ldots + A_0 \qquad (13)$$
$$A_j = \phi_{p-j}$$

According to Jury's stability criterion [12], the system is stable if and only if all roots of equation 13 are inside the unit circle, or, alternatively, if the following conditions are satisfied:

$$G(1) = A_p + A_{p-1} + \ldots + A_1 + A_0 > 0 \qquad (14)$$
$$G(-1) = A_p - A_{p-1} + \ldots - A_1 + A_0 > 0 \qquad (15)$$
$$F^+(k) = det(\hat{X}_k + \hat{Y}_k) > 0 \qquad (k = 1, 3, ..., p-1) \qquad (16)$$
$$F^-(k) = det(\hat{X}_k - \hat{Y}_k) > 0 \qquad (k = 1, 3, ..., p-1) \qquad (17)$$

$$\hat{X}_k = \begin{pmatrix} A_p & \ldots & A_{p-k+1} \\ 0 & \ddots & \vdots \\ 0 & 0 & A_p \end{pmatrix} \qquad \hat{Y}_k = \begin{pmatrix} A_{k-1} & \ldots & A_0 \\ \vdots & \ddots & 0 \\ A_0 & 0 & 0 \end{pmatrix} \qquad (18)$$

Among these criteria, the $F^-(p-1)$ parameter is found to be the most critical, since it becomes negative as any of the system's roots crosses the unit circle, as shown in [27]:

$$F^-(p-1) = A_p^{p-1} \prod_{i<j} (1 - z_i z_j) \qquad (19)$$

Torii and Matsuzaki [13] have suggested the following stability parameter formulation for a 2-DOF aeroelastic systems (binary flutter mechanism):

$$F_Z = \frac{F^-(p-1)}{F^-(1)^2} \qquad (20)$$

This parameter was shown to vary as a linear function of the dynamic pressure.

2.1.1 ARX/ARMAX Models

Similarly to the ARMA model development, a more general model that depends on an exogenous, known, signal source, additionally to the unknown random source, may be identified as the following ARMAX(p, q, m) model:

$$y_i + \phi_1 y_{i-1} + \ldots + \phi_p y_{i-p} = \epsilon_i + \theta_1 \epsilon_{i-1} + \ldots + \theta_q \epsilon_{i-q} + \eta_1 u_i + \eta_2 u_{i-1} + \ldots + \eta_{m+1} u_{i-m} \qquad (21)$$

where u_i is the exogenous signal and η_i are its corresponding coefficients. Removing the MA part from ARMAX results in the following ARX(p, m) model:

$$y_i + \phi_1 y_{i-1} + \ldots + \phi_p y_{i-p} = \epsilon_i + \eta_1 u_i + \eta_2 u_{i-1} + \ldots + \eta_{m+1} u_{i-m} \qquad (22)$$

for both ARMAX and ARX models, eq. 13 to 20 still hold, as the characteristic equation depends solely on the AR coefficients.

2.1.2 Parameter Estimation

In the current study, the ARMA/ARX/ARMAX model coefficients ϕ_i, θ_i, η_i and the noise variance σ^2 are computed using the MATLAB System Identification Toolbox armax.m function.

2.1.3 Roots Classification

From equation 6, it is observed that since $\Delta t \ll 1$, the characteristic roots are typically located close the unit circle on the first and fourth quarters of the complex plane. Figure 1(a) presents an illustration of the typical dispersion of an ARMA model characteristic roots for a binary flutter mechanism case (p=4).

Considering a single flutter test point at constant flow conditions, estimating multiple structural response samples of the investigated system should, theoretically, result in identical root locations in the z-plane. Multiple samples may be obtained by using different accelerometers and/or signal segmentation. In reality, some samples result in poor estimations than others, as demonstrated in figure 1(b) for a case of multiple sample estimations at constant flow conditions at which the aeroelastic system is stable. A group of "proper" root estimations is identified inside the unit circle, while a few poor estimations are located outside the unit circle or away from the group centroid. Poor estimations may result from any temporary deviation from the estimation model assumptions, such as non-random excitation, colored (not white noise) excitation, insufficient structural response or local flow phenomena. To address these cases, the following classification procedure is suggested in order to identify the "proper" set of estimations from a given set of root estimations in the z-plane and a tolerance parameter tol:

1. Root estimations outside the unit circle are identified and eliminated
2. A centroid z_μ is evaluated by the remaining root locations
3. The variance z_σ is identified for each root location by its distance from z_μ
4. If $max(z_\sigma) > tol$, the most distant root estimation is eliminated
5. The process is repeated until $max(z_\sigma) \leq tol$

According to this procedure, the proper set of roots is circumscribed by a circle of tol radius, as illustrated in Figure 1(b). This post-processing procedure was previously suggested and studied by the authors in [28]. A parametric investigation which was conducted in this study has shown little dependency of the procedure performances on the classification tolerance values. This procedure is used in the current study for all ARX/ARMA/ARMAX estimations to generalize the ARMA estimations from multiple accelerometers measurements into a global system model. The procedure also enables statistical evaluation of the estimation variance bounds, as presented in the current study.

2.2 Operational Modal Analysis Model

For a N_m-DOF system with multiple N_i inputs and N_o outputs, the system frequency response function (FRF) is given by:

$$H(\omega) = S_{YF}(\omega) S_{FF}^{-1}(\omega) \in \mathbb{C}^{N_o \times N_i} \tag{23}$$

where $S_{YF} \in \mathbb{C}^{N_o \times N_i}$ and $S_{FF} \in \mathbb{C}^{N_i \times N_i}$ are the cross and auto spectra of the input and output signals F and Y, respectively. The FRF may be decomposed into the following Laplace-domain pole-residue modal model [29]:

$$H(\omega) = \sum_{r=1}^{N_m} \frac{\Phi_r L_r^T}{i\omega - s_r} + \frac{\Phi_r^* L_r^H}{i\omega - s_r^*} \tag{24}$$

where s_r, Φ_r and L_r are the modal Laplace parameter, mode shape and participation factor of the r-th mode, respectively, $*$ denotes complex conjugate, $(\cdot)^H$ is the transpose complex conjugate

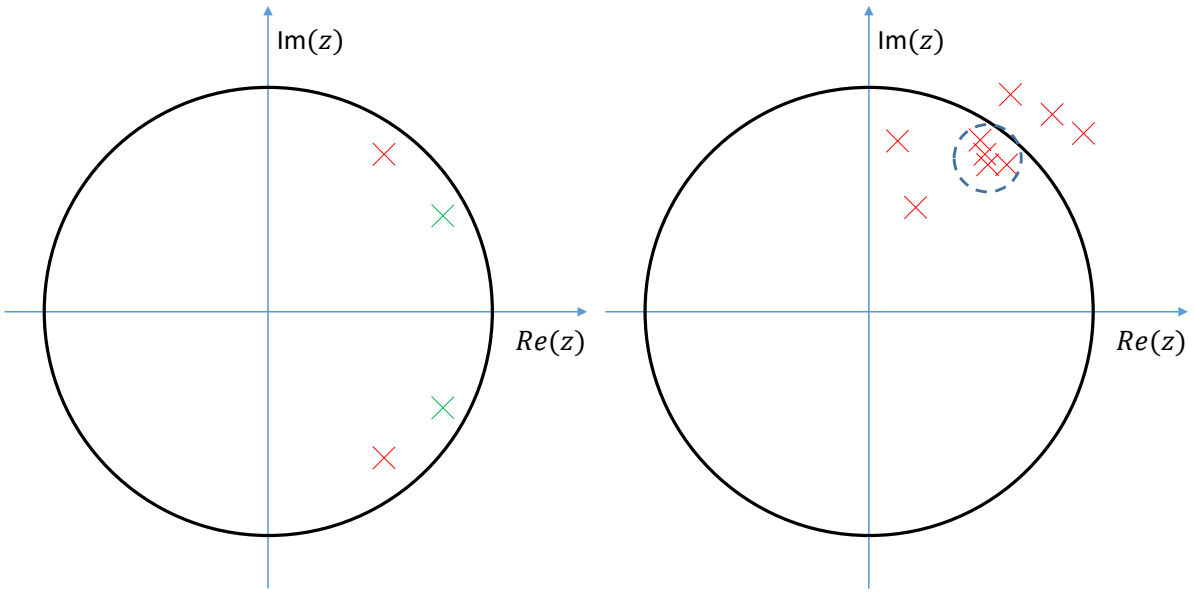

(a) Single sample estimation (all roots) (b) Multiple sample estimation (single root)

Figure 1: Typical dispersion of characteristic equation roots in the complex z plane

(Hermitian) operator and $(\cdot)^T$ is the transpose operator. As shown in [30], if the excitation forces may be considered stationary stochastic processes, the following relation between the input and output power spectra functions $S_{YY}(\omega)$ and $S_{FF}(\omega)$ holds:

$$S_{YY}(\omega) = H(\omega) S_{FF}(\omega) H(\omega)^H \tag{25}$$

Further assuming that the excitation signals are normally distributed white noise signals, $S_{FF}(\omega)$ may be considered a constant matrix with respect to the frequency, thus substituting 24 into 25 we obtain:

$$S_{YY}(\omega) = \sum_{r=1}^{N_m} \frac{\Phi_r Q_r^T}{i\omega - s_r} + \frac{\Phi_r^* Q_r^H}{i\omega - s_r^*} + \frac{\Phi_r Q_r^T}{-i\omega - s_r} + \frac{\Phi_r^* Q_r^H}{-i\omega - s_r^*} \tag{26}$$

where Q_r is the modal reference vector for the r-th mode. The similarity between the FRF (24) and S_{YY} (26) modal models suggests that parametric models that are used for the estimation of the FRF matrix may also be used for the estimation of S_{YY}, with the only difference of model order required to obtain the N_m system modal parameters. The output power spectra function may be calculated directly from the structural response signals Fourier transform $\hat{Y}(\omega) \in \mathbb{C}^{1 \times N_o}$ using the Welch periodogram method [31]:

$$S_{YY}(\omega) = \frac{1}{N_b} \sum_{j=1}^{N_b} \hat{Y}_j^{ref} \hat{Y}_j^H \in \mathbb{C}^{N_o \times N_{ref}} \tag{27}$$

where $\hat{Y}^{ref}$ is the Fourier transform of a set of N_{ref} output signals that are used as reference signals. The signals spectra are averaged over N_b segments. The power spectra covariances may be similarly evaluated by:

$$cov(S_{YY}) = \frac{1}{N_b - 1} \sum_{j=1}^{N_b} |\hat{Y}_j^{ref} \hat{Y}_j^H - S_{YY}|^2 \in \mathbb{C}^{N_{ref} \times N_o} \tag{28}$$

The following sections describe MIMO parametric estimation models used for modal parameters extraction based on the output power spectra functions within the OMA method. Once the estimation models are outlined, the FM stability parameter is identified.

2.2.1 Poly-reference least square complex frequency model (pLSCF)

According to this model, the S_{YY} matrix is modeled by:

$$\hat{S}_o(\omega) = N_o(\omega)D(\omega)^{-1}, o = 1..N_o \tag{29}$$

$$N_o(\omega) = \sum_{j=0}^{n} e^{-i\omega\Delta tj} B_{oj} \tag{30}$$

$$D(\omega) = \sum_{j=0}^{n} e^{-i\omega\Delta tj} A_j \tag{31}$$

where $B_{oj} \in \mathbb{R}^{1\times N_{ref}}$ and $A_j \in \mathbb{R}^{N_{ref}\times N_{ref}}$ are the real-valued coefficients to be estimated. Each element in the $\hat{S}_o(\omega) \in \mathbb{C}^{N_o\times N_{ref}}$ matrix represents a different combination of reference/output spectra. This poly-reference implementation models the relation between each output to all reference signals as a matrix fraction, while global modal parameters may be obtained for all spectra using eigenvalue decomposition of the so-called companion matrix, which is based on A, as presented in [17]. For this model, the following linearized quadratic cost function is identified:

$$l_{pLSCF} = \sum_{o=1}^{N_o}\sum_{f=1}^{N_f} trace(E_o^H(\omega_f)E_o(\omega_f)) = E_o(\omega_f)E_o^H(\omega_f) \tag{32}$$

$$E_o(\omega) = W_o(\omega)(N_o(\omega) - \hat{S}_o(\omega)D(\omega)) \tag{33}$$

The estimation process may be obtained using a linearized, weighted, LS technique for which the following cost function formulation and Jacobian matrix are identified:

$$l_k = \begin{Bmatrix} \epsilon_k(\omega_1) \\ \vdots \\ \epsilon_k(\omega_{N_f}) \end{Bmatrix} = [J]\{\theta\} = \begin{bmatrix} \Gamma_k & \Phi_k \end{bmatrix} \begin{Bmatrix} vec(B_k) \\ vec(A) \end{Bmatrix} \tag{34}$$

$$\Gamma_o = \begin{bmatrix} W_o(\omega_1)[e^{-i\omega_1\Delta t0} \dots e^{-i\omega_1\Delta t0}] \otimes I_{N_i} \\ \vdots \\ W_o(\omega_{N_f})[e^{-i\omega_{N_f}\Delta tn} \dots e^{-i\omega_{N_f}\Delta tn}] \otimes I_{N_i} \end{bmatrix} \tag{35}$$

$$\Phi_o = \begin{bmatrix} -W_o(\omega_1)[e^{-i\omega_1\Delta t0} \dots e^{-i\omega_1\Delta t0}] \otimes \hat{S}_o(\omega_1) \\ \vdots \\ -W_o(\omega_{N_f})[e^{-i\omega_{N_f}\Delta tn} \dots e^{-i\omega_{N_f}\Delta tn}] \otimes \hat{S}_o(\omega_{N_f}) \end{bmatrix} \tag{36}$$

The pLSCF estimator supports the capability to obtain stabilization diagrams directly from a single model estimation iteration, as demonstrated in the results section. In these charts, the model order may be varied as part of a single model estimation iteration, enabling for physical pole estimates to be distinguished from numerical artifacts.

2.2.2 Maximum likelihood estimator (pMLE)

The presented pLSCF model is considered purely deterministic as long as the weighting function $W(\omega)$ is not related to any probabilistic characteristic of the measurements. To improve the estimation performances with regard to noise effects, the following ML stochastic model was suggested [17]. Following the pLSCF formulation (eq. 29), the non-linear cost function is identified as:

$$l_{pMLE} = \sum_{o=1}^{N_o} \sum_{f=1}^{N_f} E_o^{pML^*}(\omega_f) C_o^{-1}(\omega_f) E_o^{pML^T}(\omega_f) \tag{37}$$

$$E_o^{pML}(\omega_f) = \hat{S}_o(\omega_f) - N_o(\omega_f) D^{-1}(\omega_f) \tag{38}$$

where $(\cdot)^*$ is the complex conjugate and $C_o \in \mathbb{R}^{N_i \times N_i}$ is the covariance matrix of the output related power spectra, obtained as a diagonal matrix based on the relevant elements from $cov(S_{YY})$(eq. 28). Gauss–Newton optimization iterations may be applied to this model as well, as suggested by Cauberghe [17]. The computational effort required in a single pMLE iteration equals to approximately N_{ref}^3 times the effort required for a full pLSCF estimation process.

2.2.3 Iterative quadratic maximum likelihood parametric estimator (pIQML)

While the pMLE estimator offers enhanced capabilities for low signal-to-noise ratio measurements compared with pLSCF, the need in multiple iterations to obtain a single model estimation may lead to impractical computational time or memory demands, especially if near real-time estimation is required or large number of sensors are being used. Furthermore, pMLE does not support the capability to obtain stabilization diagrams directly from a single model estimation iteration, which is an important practical disadvantage. IQML estimators suggest a compromise between pLSCF efficiency and pMLE precision characteristics by using a stochastic parametric weighting function $W = f(cov(\hat{S}), A, B, \omega)$ within the pLSCF formulation, which enables near-pMLE precision characteristics while maintaining the overall advantages of the pLSCF estimator.

For the poly-reference implementation (pIQML), an adequate weighting function takes the following form:

$$W_o^2(A, \omega) = \frac{1}{trace(D^H(A, \omega) C_o(\omega) D(A, \omega))} \tag{39}$$

which corresponds to the following cost function:

$$l_{pIQML} = \sum_{o=1}^{N_o} \sum_{f=1}^{N_f} \frac{E_o(\omega_f) E_o^H(\omega_f)}{trace(D^H(A, \omega_f) C_o(\omega_f) D(A, \omega_f))} \tag{40}$$

In [17, 19] it is shown that by using this formulation of the weighting function, the cost function converges into the pMLE cost function identified in equation 37. A converged weighting function may typically be obtained within a few iterations of the LS solution.

2.2.4 Parameter Estimation

A combination of these OMA estimation models was suggested by El-Kafafy et al. [32] as the PolyMax-Plus estimator, which is available within the LMS International experimental structural dynamics commercial tool. In the current study, the pIQML estimator was implemented

into an in-house MATLAB code and used for modal parameters estimation. Since this implementation enables a SIMO estimation of the modal parameters, no post-processing procedures are required to obtain a global model from the multiple accelerometers data.

2.2.5 Flutter margin stability parameter (FM)

For a 2-DOF dynamic system, the characteristic equation in the laplace domain is a quartic equation of the form:

$$\lambda^4 + A_3\lambda^3 + A_2\lambda^2 + A_1\lambda + A_0 = 0 \tag{41}$$

The system remains stable according to the Routh-Hurwitz criterion if

$$[(A_2/2)^2 - A_0] - [A_2/2 - A_1/A_3] > 0 \tag{42}$$

Equation 41 roots are the two laplace variables identified in equation 3 and their complex conjugates:

$$\lambda_{1,3} = \zeta_1\omega_1 \pm i\omega_1 \tag{43}$$
$$\lambda_{2,4} = \zeta_2\omega_2 \pm i\omega_2 \tag{44}$$

By identifying eq. 41 coefficients from the system roots we obtain:

$$A_3 = -2(\zeta_1\omega_1 + \zeta_2\omega_2) \tag{45}$$
$$A_2 = \zeta_1^2\omega_1^2 + \zeta_2^2\omega_2^2 + \omega_1^2 + \omega_2^2 + 4\zeta_1\omega_1\zeta_2\omega_2 \tag{46}$$
$$A_1 = -2\left[\zeta_1\omega_1(\zeta_2^2\omega_2^2 + \omega_2^2) + \zeta_2\omega_2(\zeta_1^2\omega_1^2 + \omega_1^2)\right] \tag{47}$$
$$A_0 = \zeta_2^2\omega_2^2 + \omega_2^2 + \zeta_1^2\omega_1^2 + \omega_1^2 \tag{48}$$

Substituting 45 into 42 results in a parameter identified by Zimmerman and Weissenburger [1] as the flutter margin stability parameter:

$$FM = \frac{1}{4}\left[\omega_2^2 - \omega_1^2 + \zeta_2^2\omega_2^2 - \zeta_1^2\omega_1^2\right]^2 + 2\zeta_1\omega_1\zeta_2\omega_2\left[\omega_1^2 + \omega_2^2 + (\zeta_1\omega_1 + \zeta_2\omega_2)^2\right] \tag{49}$$
$$-\frac{1}{4}\left[\frac{\zeta_2\omega_2 - \zeta_1\omega_1}{\zeta_1\omega_1 + \zeta_2\omega_2}(\omega_2^2 - \omega_1^2) + (\zeta_1\omega_1 + \zeta_2\omega_2)^2\right]^2 \tag{50}$$

Once the modal parameters are estimated using the pIQML estimator, the FM stability parameter may be evaluated and extrapolated as a quadratic function of the dynamic pressure to predict the instbaility onset conditions. Price and Lee [9] have developed an extended version of the FM parameter for trinary flutter mechanisms.

3 PREVIOUS INVESTIGATION

In a previous study by the authors [28], the ARMA method was used to process structural responses to natural air turbulence excitation measurements obtained in Israel Air Force (IAF) flutter flight test campaigns of a subsonic UAV platform, as well as the F-15 and F-16 platforms at transonic flow conditions. These tests were conducted using traditional flutter methods and not specifically designed for the purpose of AFFTTs assessment, therefore test procedures were not optimized in terms of recording time, amount of test points at constant aeroelastic characteristic conditions, and the lack of a reliable instability boundary reference identifications.

Nevertheless, the ARMA model predictions obtained in this study were able to support the feasibility of applying this method for various real-life flutter test cases. The presented roots classification method was applied to obtain proper assessment of the stability parameter based on multiple data samples from several sensors and/or measurements at nearby dynamic pressure conditions. This procedure, as well as signal processing techniques such as re-sampling and filtering, were investigated and optimized in this study. In the current study, similar procedures are applied during the ARMA/ARMAX/ARX model evaluations. Figure 2 presents estimated F_Z stability parameter and modal frequency variations with normalized dynamic pressure at $M = 0.7$ and $M = 0.75$ for the F-16 platform test case presented in [28]. Variance bounds are evaluated based on the roots classification procedure standard deviations. These results indicate that linear trends of the estimated stability parameter with dynamic pressure may in-fact be achieved. This test case configuration and flutter mechanism characteristics are generally similar to the current study test case, therefor these results are used as a baseline for the current study.

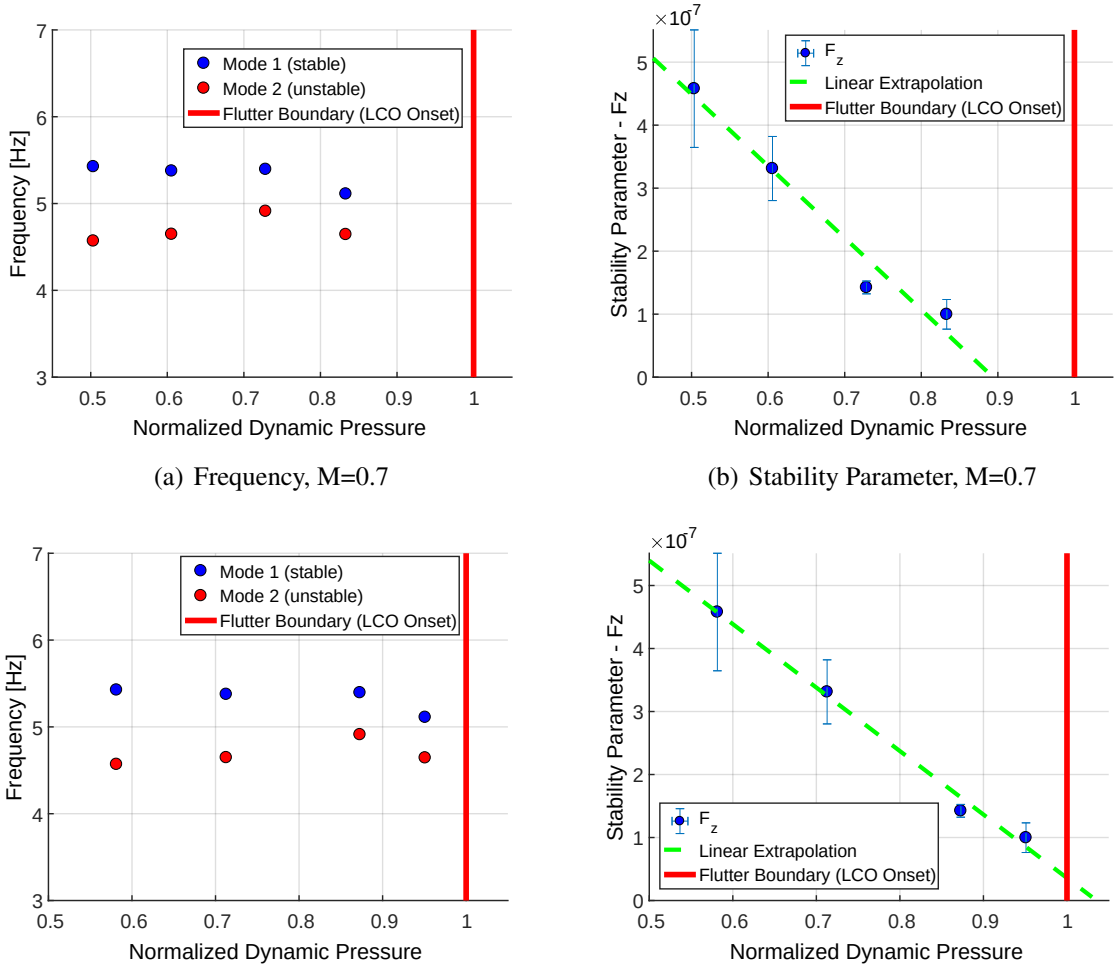

(a) Frequency, M=0.7

(b) Stability Parameter, M=0.7

(c) Frequency, M=0.75

(d) Stability Parameter, M=0.75

Figure 2: ARMA model evaluation for the F-16 platform, reproduced from [28]

4 FLUTTER FLIGHT TEST CASE

Figure 3 shows the F-16 flutter flight test configuration used in the current study. It consists of three fuel tanks at inboard stations, two $2000\,lb$ stores and two outboard air-to-air missiles. The configuration is fully symmetric. During the flutter test procedures, both underwing fuel tanks were maintained full. This configuration was chosen due to previous flight test indication of low modal dampings and moderate Limit Cycle Oscillation (LCO) responses observed at transonic flow conditions. As the F-16 LCO phenomenon is generally considered a nonlinear evolution of flutter instability [33, 34] and typically occurs at flow conditions close to flutter onset, the appearance of LCO is a favorable characteristic of this configuration for the purposes of the current study. It enables possible penetration of the flutter/LCO onset boundary during the test into the dynamically unstable region, as long as LCO response levels remain within acceptable limits. In the current study, this capability is exploited to obtain a reliable experimental evaluation of the instability boundary, which is then used as reference for the AFFTTs evaluation. According to the available data on the test configuration, from both flight tests and linear anal-

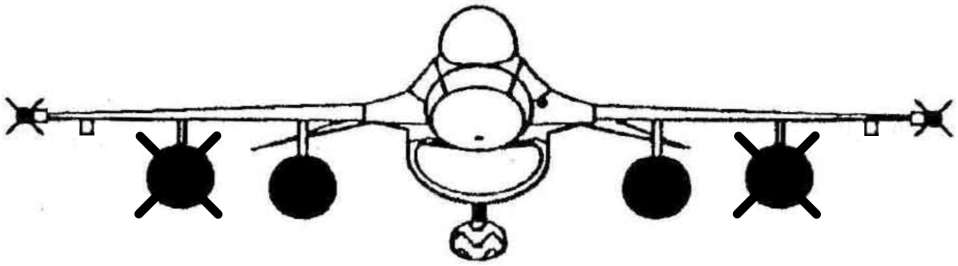

Figure 3: F-16 flutter flight test configuration

ysis, its critical flutter mode may be characterized as an anti-symmetric mechanism in which an outboard wing fore-torsion mode of $5.8\,Hz$ frequency couples with a wing bending mode of $5.0\,Hz$ frequency. The flutter frequency is $5.4\,Hz$, as the torsion mode becomes unstable.

Figure 4 presents linear flutter analysis results obtained for the test configuration by means of traditional $\omega - V - g$ charts, in which negative modal dampings correspond to stable dynamic characteristics. This analysis was performed using an in-house matched-point flutter G solver at $M = 0.8$ using linear panel aerodynamic model. Since a structural modal damping model was unavailable for this configuration, the analysis assumes constant $g = 2\%$ damping ratios for all mode shapes. Consequently, the dynamic pressure in fig. 4 is normalized by the analytic flutter onset dynamic pressure, thus enabling a more straight-forward comparison with the flight test data. In this analysis, modes 2 and 4 correspond to the stable and unstable flutter mechanism modes, respectively.

5 FLIGHT TEST PROCEDURE

Flight test data was collected in a single sortie during which all test points were conducted at constant Mach number conditions of $M = 0.8$ and varying altitudes. For each test point, after stabilizing at 1-g level flight at the required altitude, structural acceleration data was recorded during excitation by the following techniques:

1. Natural air turbulence excitation (termed ”turbulent excitation”)
2. White-noise random excitation applied by the pilot using the aircraft’s flaperon surfaces forced excitation system (termed ”forced excitation”)

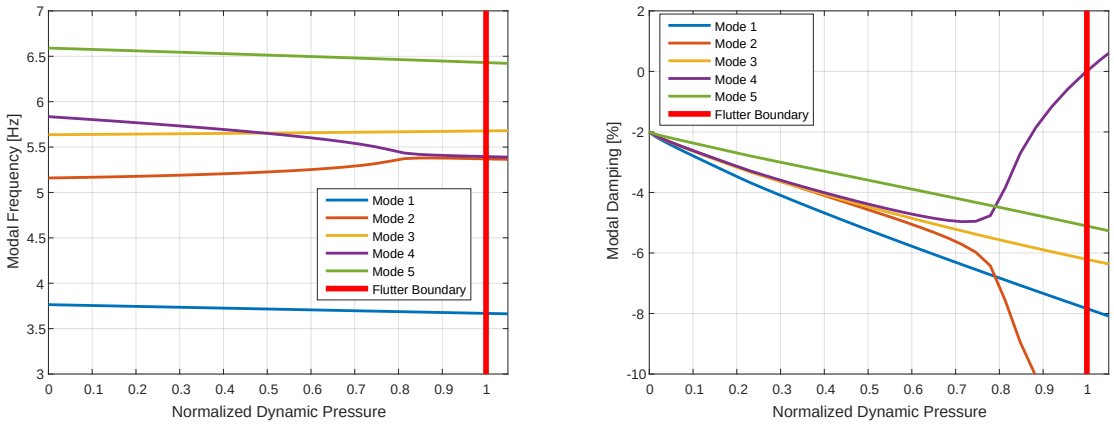

(a) Modal Frequency

(b) Modal Damping

Figure 4: $\omega - V - g$ charts from linear flutter analysis of the test configuration, $M = 0.8$

Both excitation techniques were applied for $30 - 60$ second periods, while structural responses were monitored using four accelerometers located at the wingtip launchers. The acceleration data was recorded at $500\,Hz$ sampling frequency. As the flight altitude was decreased (dynamic pressure increased), the instability boundary was approached, until at some conditions, the structural responses after the forced excitation was stoped did not decay, and LCO responses were identified. These conditions were then further investigated to better identify the LCO onset conditions.

Figures 5 to 9 present a comparison between the different test points (TPs) in terms of flow conditions variation (fig. 5), wingtip accelerations and flaperon deflections (fig. 6), structural responses spectrograms (fig. 7) and periodograms (fig. 8), as well as the coherence function between the wingtip accelerations and flaperon positions (fig. 9). In all cases, the solid and dashed lines correspond to turbulent and forced excitation test points, respectively. Figure 5 shows the four TPs of various data recording length obtained using each excitation technique, with most data falling in the tolerances of $M = 0.8 \pm 0.01$ and $q/q_{ref} = [0.8, 0.9, 0.95, 1] \pm 0.03$. To eliminate the effects of non-negligible variations in dynamic pressure on the stability parameter characteristics, the signals were divided into several segments. Although improving the flow conditions tolerances, this segmentation also unfavorably affects the model estimation procedures, as short data samples estimations tend to be more noise sensitive and therefor result in inferior results compared to long samples estimations. This trade-off in signal segmentation was optimized for each AFFTT method and excitation method, resulting in segments length raging between 15 to 25 seconds for all signals using the ARMAX estimation models, and full sample length for the OMA model, as further discussed below.

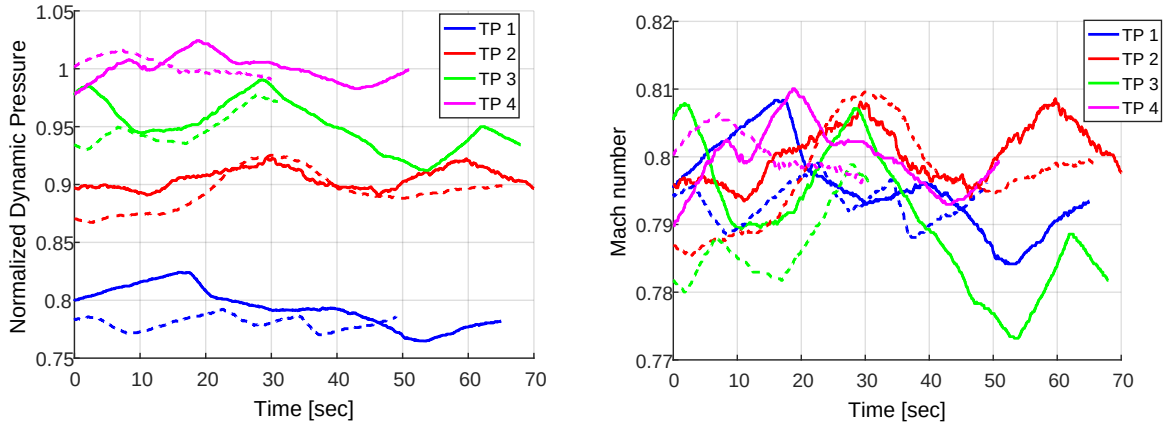

(a) Dynamic Pressure

(b) Mach number

Figure 5: Flight conditions variation during the flight test; solid line - turbulent excitation, dashed line - forced excitation

Figure 6 presents wingtip accelerations and flaperons deflection angles variations for both excitation methods. The presented data was filtered in the $[1-10]\,Hz$ band. Results indicate that flaperon deflections are approximately $2-5$ times higher for forced excitation compared with turbulent excitation, while wingtip accelerations are only approximately $1-3$ times higher. This suggests that turbulent excitation may be used as an effective means of perturbing the structure, comparable to the forced excitation. This also implies that air turbulence excitation can not be neglected in analyzing the response to forced excitation. Spectrograms and periodograms of the unfiltered acceleration signals, which are presented in figs. 7 and 8, further support these identifications, as the forced excitation frequency content strengthening is mainly visible at the low frequency band of $[2-20]\,Hz$, while for higher frequencies the power spectra levels seem comparable for both excitation methods. The coherence function between the left wing flaperon deflection angle and the corresponding wingtip accelerometer is presented in fig. 9 for the second test point. In this comparison, low coherence levels are obtained for the turbulent excitation method across the presented spectrum. This is expected, since in this case the structural response is mainly due to air turbulence rather than flaperon deflections. In the forced excitation case, low coherence is also obtained at frequencies higher than $15\,Hz$. This may be attributed to the dynamic characteristics of the flaperon servos, as the high frequency excitation signals are truncated by the servo mechanical limitations. At the lower frequency band, relatively high coherence levels are obtained, except for at specific frequencies, which generally correspond to the aeroelastic frequencies. This further indicates that the structural response to flaperon excitation is considerably affected by air turbulence.

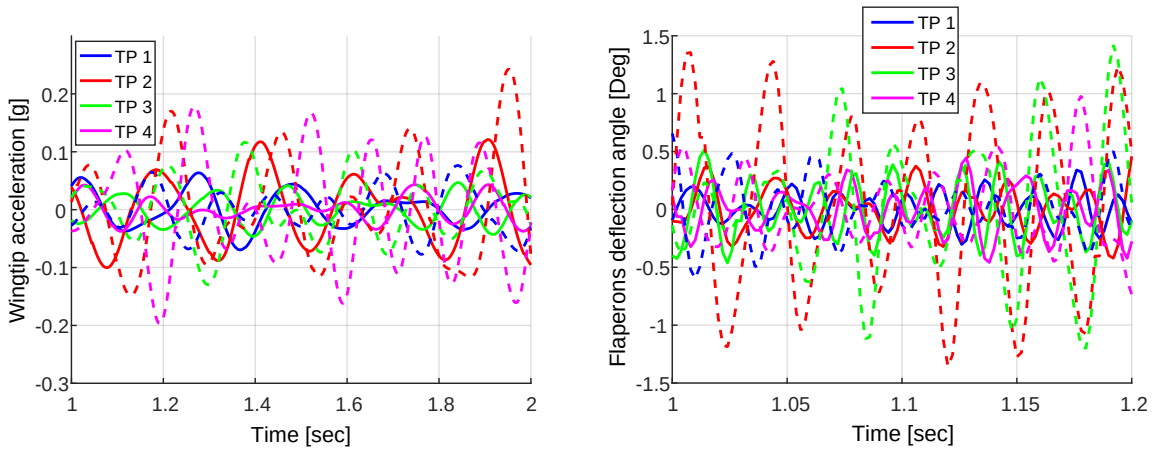

(a) Wingtip accelerations (b) Flaperons deflection angles

Figure 6: Flaperon deflections and wingtip accelerations variation during the flight test; solid line - turbulent excitation, dashed line - forced excitation

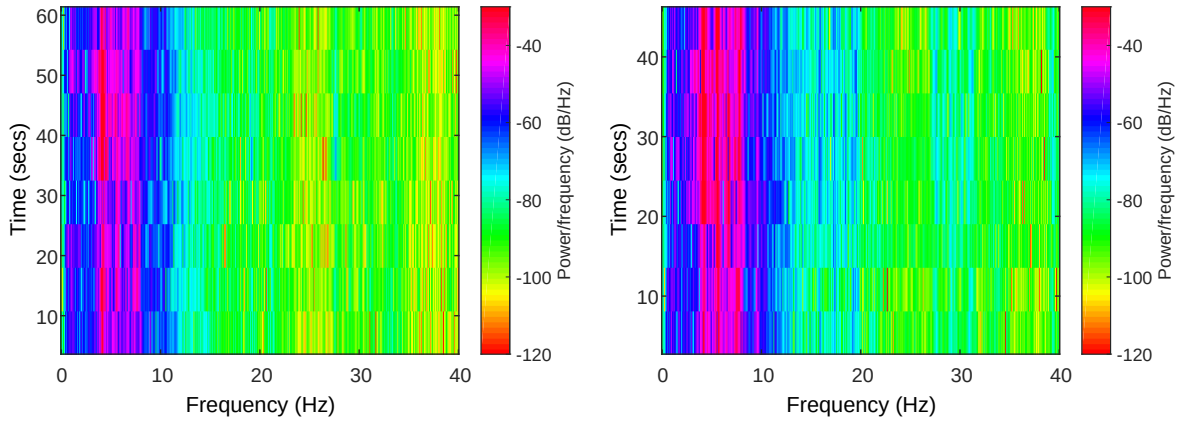

(a) Turbulent excitation (b) Forced excitation

Figure 7: Wingtip acceleration response spectrogram during TP 1 excitations

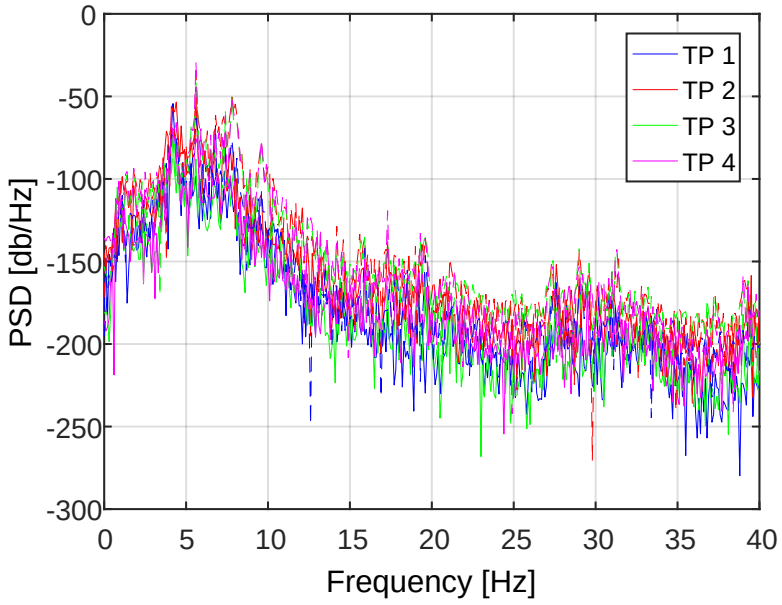

Figure 8: Wingtip acceleration responses periodograms; solid line - turbulent excitation, dashed line - forced excitation

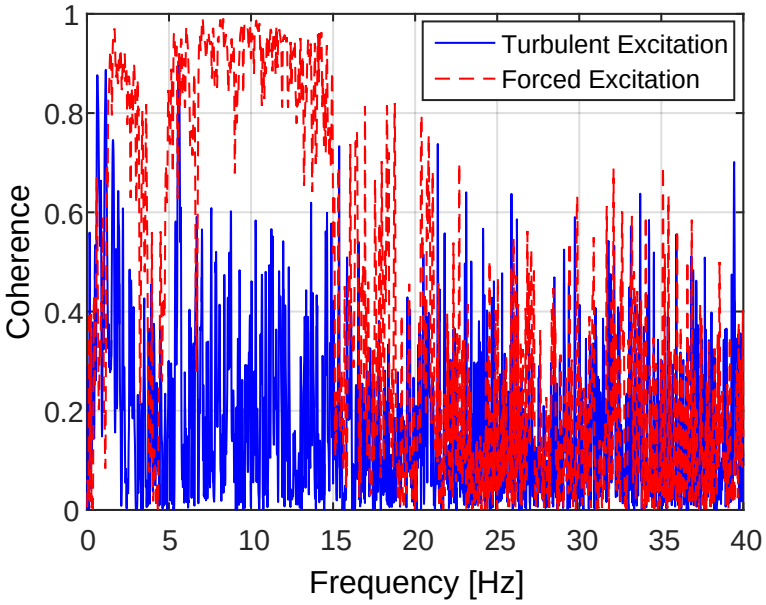

Figure 9: Left wingtip acceleration to flaperon deflection angle coherence functions, TP 2; solid line - turbulent excitation, dashed line - forced excitation

6 INSTABILITY ENVELOPE PREDICTION

6.1 ARMA/ARMAX/ARX Estimation

Figures 10 to 13 present stability parameters estimations using the ARMA, ARMAX and ARX models for the turbulent and forced excitations data. All evaluations presented in this section are based on the acceleration signals after they were filtered using a 4^{th} order butterworth filter

in the band of $[4.5 - 6.5]\,Hz$. In all estimations, the AR model order is set to $p = 4$, which corresponds to a 2-DOF dynamic system, while the MA and/or X orders are set to $q = p - 1$ or determined by the AIC minimization method. This determination of the AR model order assumes that the flutter mechanism characteristics may be well identified using a binary modal model. In all estimations, multiple accelerometers and signal segments from nearby dynamic pressure conditions are averaged using the roots classification procedure using $tol = 2 \times 10^{-3}$. The presented confidence bounds of the stability parameters represent the standard deviation of each data point based on the population of all available proper estimations within an equivalent air speed range of $1\,Kts$.

Figure 10 presents the estimated frequency and stability parameter variations with dynamic pressure for the turbulent excitation data cases using an ARMA$(p = 4, q = 3)$ model. The estimated modal frequencies are in good agreement with the linear analysis predictions (see fig. 4a). In this case, the F_z stability parameter presented in fig. 10b follows the expected linear decrease with dynamic pressure. Furthermore, extrapolation of this linear trend to a zero value dynamic pressure, which represent the instability onset condition, agrees well with the LCO onset condition that was identified in the flight test (indicated by the red line).

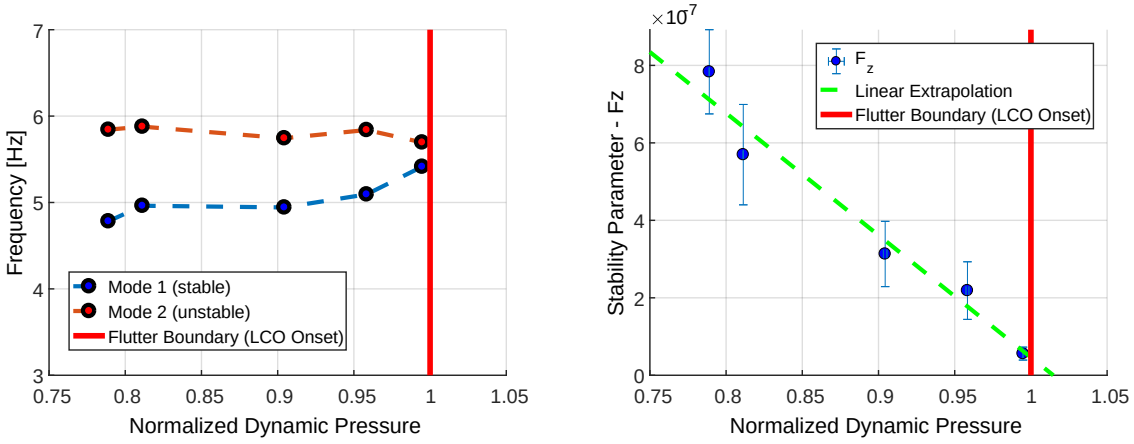

(a) Modal Frequency

(b) Stability Parameter

Figure 10: Estimated modal frequencies and stability parameter, turbulent excitation data cases; ARMA$(p = 4, q = 3)$ model

Similar results are presented in fig. 11 for a case in which the AIC minimization technique was used to determine the MA orders according to $q^{opt} = \arg\left[\min AIC\right]$. Using this technique, optimal MA orders in the range of $[3-30]$ were identified for the different segments. Nevertheless, results indicate that the MA order effect on the estimated frequency and stability characteristics is minor.

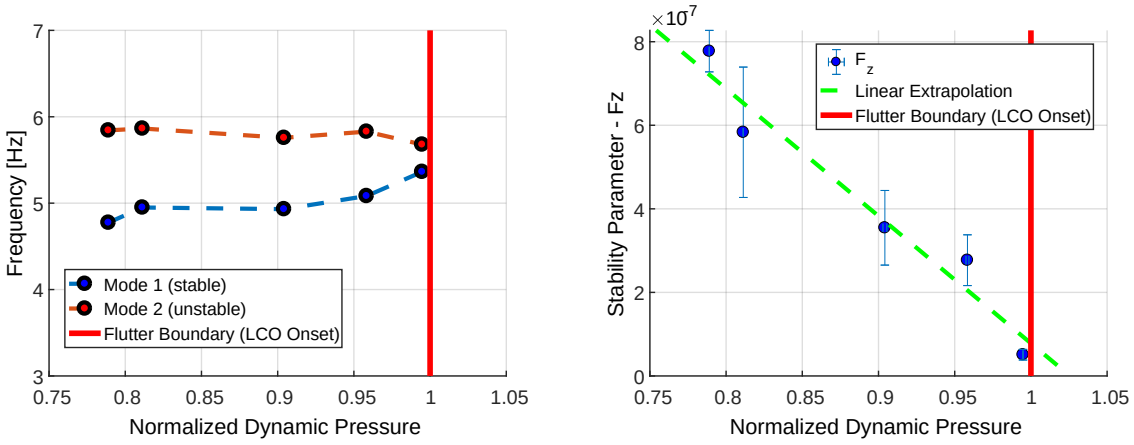

(a) Modal Frequency

(b) Stability Parameter

Figure 11: Estimated modal frequencies and stability parameter, turbulent excitation data cases; ARMA($p = 4, q = q^{opt}$) model

As demonstrated in figs. 7 to 9, structural responses to forced excitation are considerably affected by the presence of turbulent excitation. This raises a dilemma regarding of proper ARMAX modeling for the forced excitation data. Using the ARX and ARMA models seems generally unjustified, as they assume either single deterministic (X) or stochastic (MA) excitation sources. From this point of view, the full ARMAX model seems more appropriate for the current test case characteristics. Figures 12 and 13 present stability parameter estimations for the forced excitation data points using the ARMA, ARX and ARMAX models with constant AR model orders of $p = 4$ and constant MA/X orders of $q = m = 3$ (fig. 12) or optimal MA/X orders according to $[q^{opt}, m^{opt}] = \arg[\min AIC]$ (fig. 13). It is seen that the ARX and ARMA stability parameter estimations are more scattered in this case compared to the turbulent excitation case. The ARMA model does not provide a linear trend and therefor can not be used for instability onset prediction (see fig. 12a and fig. 13a), while the ARX model is considerably more sensitive to the model order m, as indicated by comparison of fig. 12b and fig. 13b. The ARMAX model provides the best estimation capabilities with fairly good prediction of the instability onset conditions and relatively low sensitivity to MA/X order selection, as seen in fig. 12c and fig. 13c.

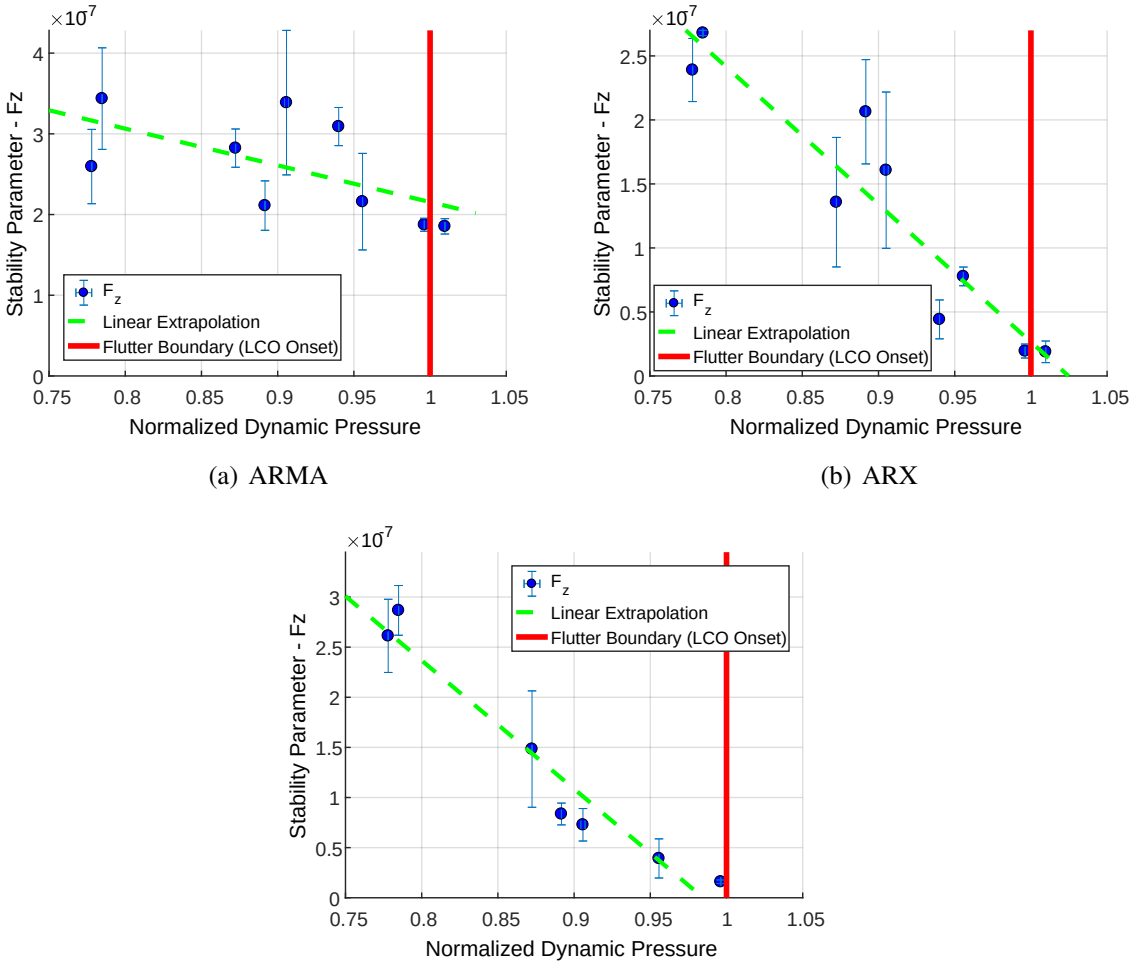

(a) ARMA

(b) ARX

(c) ARMAX

Figure 12: Estimated modal frequencies and stability parameters, forced excitation data cases; ARMA$(p = 4, q = 3)$, ARX$(p = 4, m = 3)$ and ARMAX$(p = 4, m = 3, q = 3)$ models

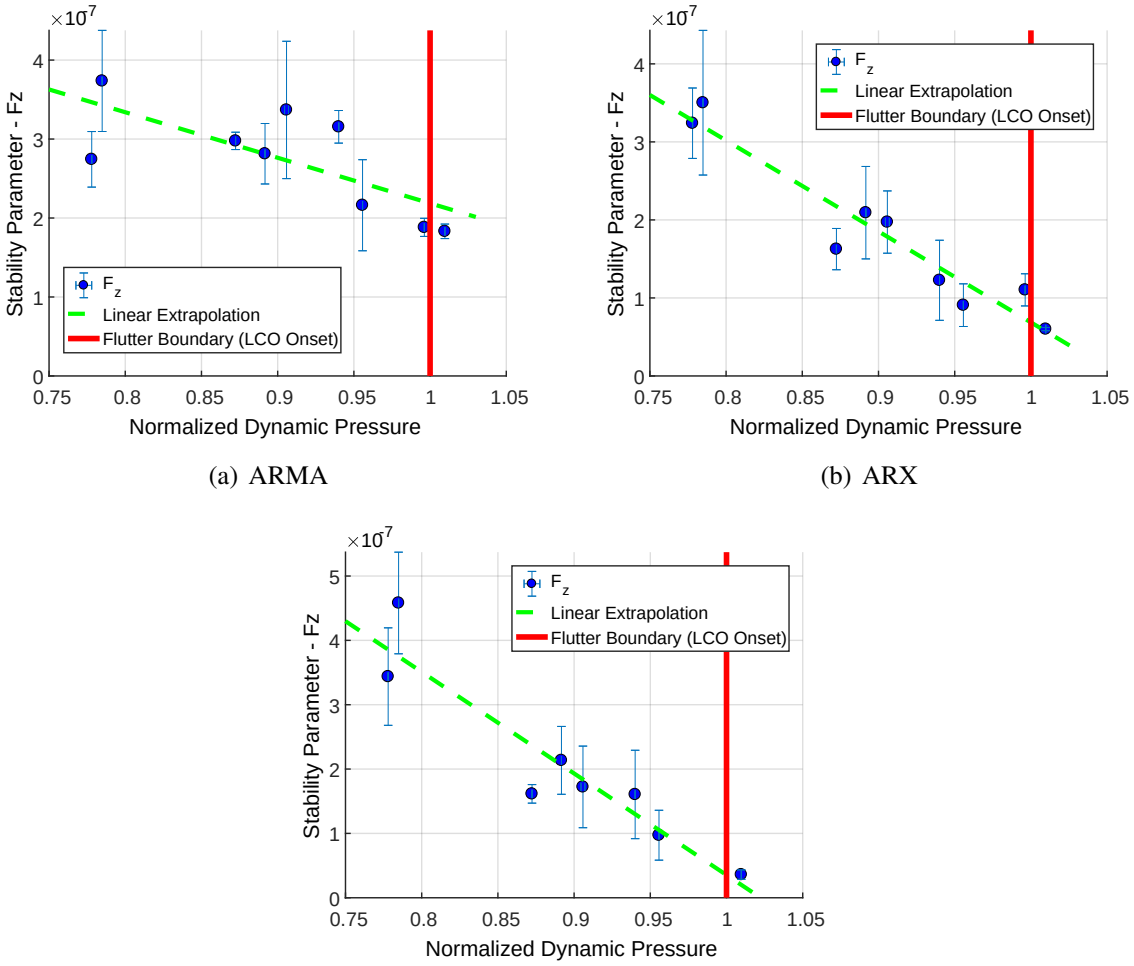

(a) ARMA

(b) ARX

(c) ARMAX

Figure 13: Estimated modal frequencies and stability parameters, forced excitation data cases; ARMA($p = 4, q = q^{opt}$), ARX($p = 4, m = m^{opt}$) and ARMAX($p = 4, m = m^{opt}, q = q^{opt}$) models

6.2 OMA Estimation

OMA estimations were conducted in two main steps: non-parametric estimation of the power spectra and power spectra covariance matrices according to the periodogram method, and poly-reference parametric estimation according to the pIQML method, as described in the Theoretical Background section. The first part of the procedure assumes constant power spectra matrix of the excitation sources S_{XX}, which is consistent with the pure stochastic white noise excitation assumptions, similar to the ARMA model. Attempts to apply this method to the forced excitation data resulted in poor estimations, similarly to the findings presented in the previous section for the ARMA model. Consequently, only results of the turbulent excitation data points are presented in this section. It is noted that combined stochastic-deterministic excitation sources versions of the OMA method (OMAX) were developed by Cauberghe [17], but these were not implemented in the current study. Using the OMA method, the original data samples were used, without any prior filtering.

Figure 14 presents the power spectra and corresponding covariance function estimations for the third test point data. These results were obtained using segmentation of $N_b = 4$ and allowing for 90% overlap between the segments. Following the signal segmentation trade-off discussed

above, the periodogram method is highly affected by the signal time length, as it directly affects both the frequency resolution and estimation noise resistance by allowing for more segments of the signal to be used and therefore improving spectral averaging. In the current case, while the unstable mode (mode 2) is clearly estimated above noise level, mode 1 is hard to identify among the surrounding noise, which poses a serious challenge for the OMA method. To improve the estimation quality, the original data signals were not pre-segmented to decrease dynamic-pressure variations, as performed in the ARMA processing.

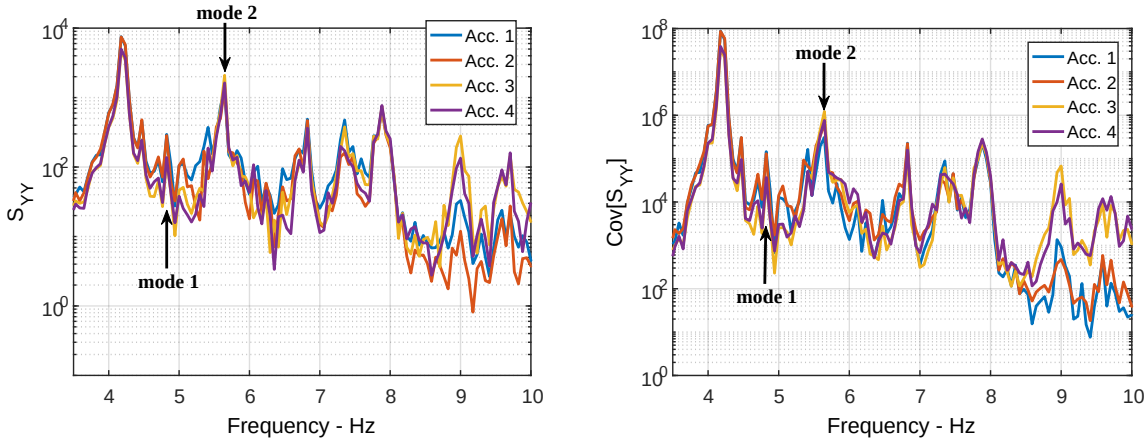

(a) Power Spectra

(b) Power Spectra Covariance

Figure 14: Non-parametric estimation of accelerations power spectra; TP3, turbulent excitation data

Figure 15 presents stability charts obtained using the pIQML estimator for the four test points. These charts identify the estimation stabilization conditions for each of the system roots as a function of model order (red stars). The unstable roots (roots with negative damping values) are omitted from these charts for the sake of simplicity. The mean S_{YY} estimation is also presented in each chart for reference purposes (blue line). For all test points the two aeroelastic flutter-related modes are identified as stable modes. However, in most cases delicate classification between relevant and non-relevant/ficticious modes is required. In the current study this was obtained effectively by identifying the relevant modes according to the mode shapes, which are estimated in a third step based on the pIQML model results.

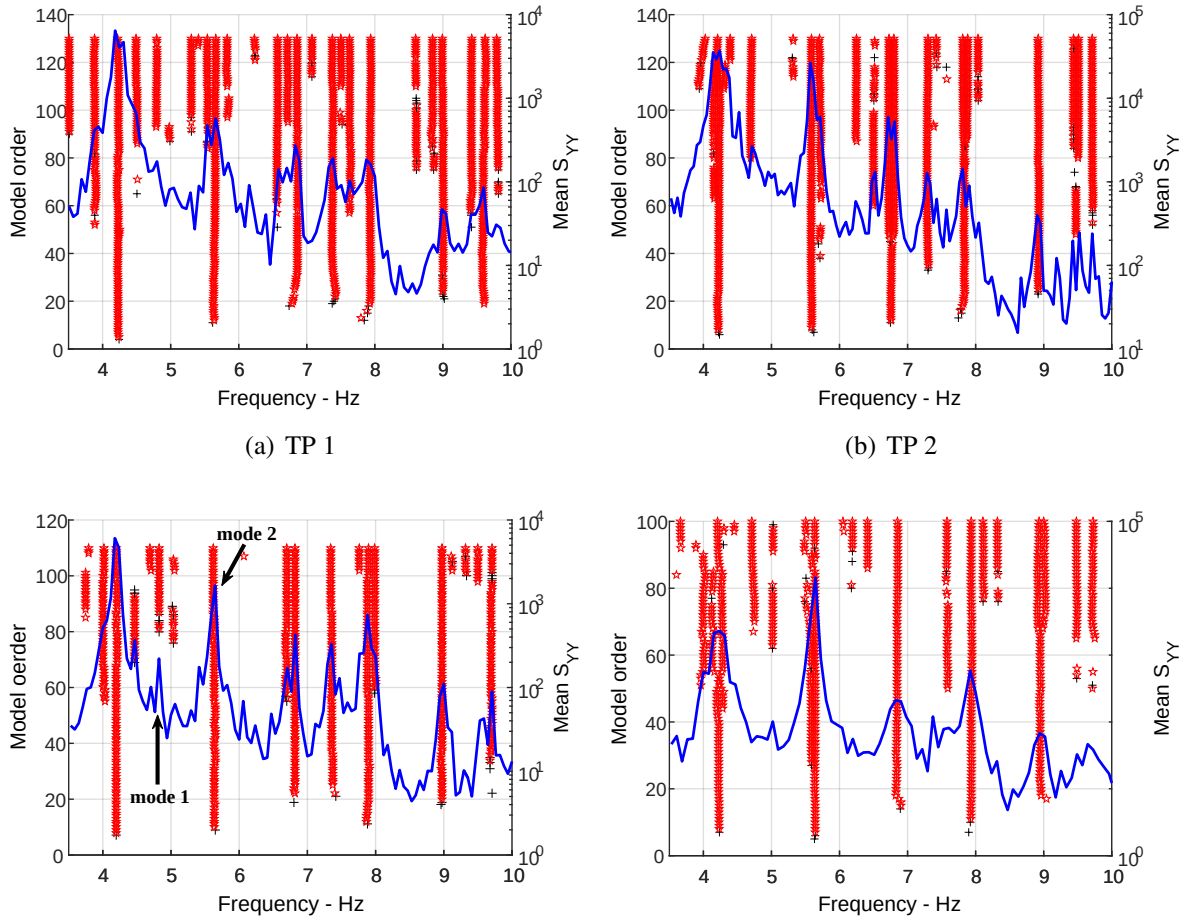

(a) TP 1

(b) TP 2

(c) TP 3

(d) TP 4

Figure 15: Stabilization diagrams, IQML estimator; turbulent excitation data. $*$ symbol - stabilized mode, $+$ symbol - stabilized frequency, unsterilized damping

Figure 16 presents the estimated modal parameters, as well as the FM stability parameter, normalized by its maximum value. In this presentation, positive damping coefficients represent stable modal characteristics (as opposed to the $\omega - V - g$ charts convention). The frequency and damping variations are in general agreement with the linear analysis presented in fig. 4, and ARMA estimations presented in fig. 10, except for two discrepancies. The OMA estimated mode 1 frequency is about $0.3\,Hz$ lower compared with the ARMA estimation, which may be related to the effect of filtering bounds on the ARMA estimation. The decrease in mode 1 modal damping is in contradiction with the linear analysis trend, as well as typical flutter mechanism behavior. It may be argued that as the the frequencies of the two modes are coalescing, the modal damping estimations of the stable mode are distorted by the unstable mode, resulting in this non-physical decrease in mode 1 damping. Nevertheless, the FM stability parameter variations with dynamic pressure presented in fig. 16c are in good agreement with the theoretical characteristics of a quadratic variation with dynamic pressure, and enable, good prediction of the instability onset conditions.

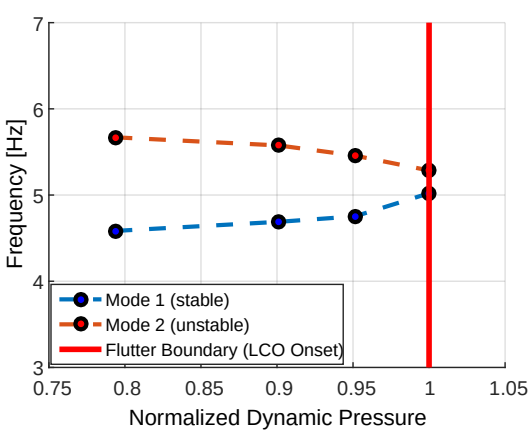

(a) Modal Frequency

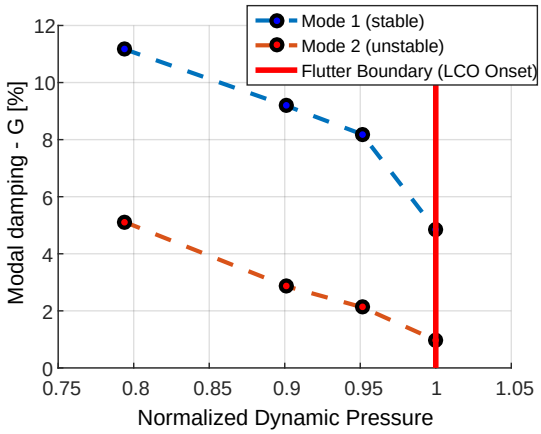

(b) Modal damping

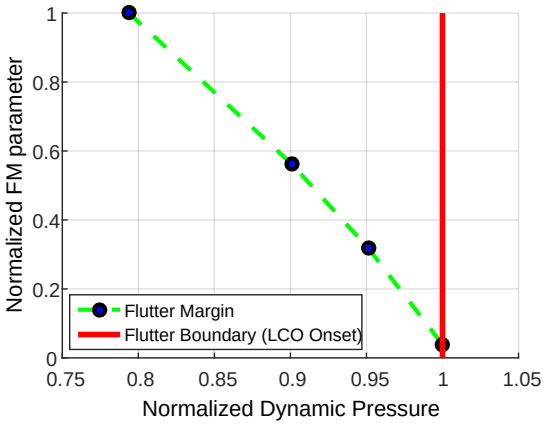

(c) Flutter Margin

Figure 16: OMA estimated modal parameters and flutter margin parameter for the test flutter mechanism, turbulent excitation test points

7 SUMMARY AND DISCUSSION

The current paper presents an assessment study for several AFFTTs including two excitation techniques, namely free air turbulence excitation and forced random excitation, two aeroelastic system identification methods, namely discrete time-series ARMAX estimators and the least-square complex frequency OMA estimator, and two corresponding flutter stability parameters, namely the F_Z and FM parameters. The assessment was conducted based on dedicated flight test data obtained on a reference configuration of the F-16 aircraft at near-LCO onset flow conditions, which are assumed to be the aeroelastic system instability onset boundaries for the purposes of this study. The aeroelastic system is identified according to the different methods assumptions and stability characteristics are investigated using the different stability parameters.

Generally speaking, all tested methods were shown to be effective for aeroelastic instability prediction, with good accuracy, under some limitations. While both excitation methods were found effective for perturbing the structural dynamics, the use of forced excitation along with system identification techniques requires the proper use of a combined deterministic-stochastic estimation approaches, such as the ARMAX model. If the test configuration is characterized by relatively lightly-damped relevant modes that may be easily perturbed using turbulent exci-

tation (as in the current study case), the use of turbulent excitation and stochastic identification methods (ARMA) may be preferable from simplicity considerations. From a practical point of view, turbulent excitation methods also have the advantage of not relying on dedicated external mechanical excitation accessories. On the other hand, the robustness of the ARMAX method when used at low subcritical dynamic pressure conditions, where the flutter modes are highly-damped, may not be addressed based on the current study test case. At such conditions, forced excitation methods may have an advantage over turbulent excitation.

From the point of view of real-time test prediction capabilities, the ARMAX method is more straight-forward and easy to implement compared with OMA, which may require delicate identification of the relevant modes. On the other hand, OMA methods have the advantage of analyzing aeroelastic systems without prior knowledge of the instability mechanism. This may be attractive in case a linear analysis in unavailable, or for purposes of analytic model calibration (rather than instability prediction). Such applications will naturally require a dedicated methodology. One requirement that is relevant to both ARMAX and OMA identification methods is for adequate data samples time length. Recording times of around 60 seconds or more are essential in order to obtain good predictions by both methods.

Based on the findings of this study, it is natural to further validate both the ARMA and OMA methods using more real-life cases. Of particular interest are the methods' performances in cases of highly-damped flutter modes or low air turbulence levels.

8 REFERENCES

[1] Zimmerman, N. H. and Weissenburger, J. T. (1964). Prediction of flutter onset speed based on flight testing at subcritical speeds. Journal of Aircraft, 1(4), 190–202.

[2] Brignac, W. J., Ness, H. B., and Smith, L. M. (1975). The random decrement technique applied to the yf-16 flight flutter tests. In AIAA 16th Structures, Structural Dynamics and Materials Conference. Reston, VA: AIAA. AIAA-1975-776.

[3] Matsuzaki, Y. and Ando, Y. (1981). Estimation of flutter boundary from random responses due to turbulence at subcritical speeds. Journal of Aircraft, 18(10), 862–868.

[4] Nissim, E. and Gilyard, G. B. (1989). Method for experimental determination of flutter speed by parameter identification. Tech. rep., NASA. TR-2923.

[5] Guillaume, P. and R. Pintelon, J. S. (1990). Description of a parametric mle in the frequency domain for mimo systems and its application to flight flutter analysis. Mechanical Systems and Signal Processing, 4(5), 405–416.

[6] Cooper, J. E., Emmett, P. R., Wright, J. R., et al. (1993). Envelope function: A tool for analyzing flutter data. Journal of Aircraft, 30(5), 785–790.

[7] Cooper, J. E. (1995). Parameter estimation methods for flight flutter testing. Tech. rep., AGARD. CP-566.

[8] Lind, R. and Brenner, M. (2000). Flutterometer: An on-line tool to predict robust flutter margins. Journal of Aircraft, 37(6), 1105–1112.

[9] Price, S. and Lee, B. (1993). Evaluation and extension of the flutter-margin method for flight flutter prediction. IEEE Transactionson Circuit Theory, 30(3), 395–402.

[10] Kehoe, M. W. (1995). A historical overview of flight flutter testing. Tech. rep., NASA. TM-4720.

[11] Routh, E. J. (1930). Advanced Part of a Treatise on the Dynamics of a System of Rigid Bodies, vol. 2. MacMillan, 5th ed.

[12] Jury, I. E. (1964). Theory and Application of the z-Transform Method. New York: Wiley.

[13] Torii, H. and Matsuzaki, Y. (2001). Flutter margin evaluation for discrete-time systems. Journal of Aircraft, 38(1), 42–47.

[14] Torii, H. and Matsuzaki, Y. (1997). Flutter boundary prediction based on nonstationary data measurement. Journal of Aircraft, 34(3), 427–432.

[15] Bae, J.-S., Kim, J.-Y., Lee, I., et al. (2005). Extension of flutter prediction parameter for multimode flutter systems. Journal of Aircraft, 42(1), 285–288.

[16] Parloo, E. (2004). Application of Frequency-Domain System Identification Techniques in the Field of Operational modal Analysis. Ph.D. thesis, Vrije University, Brussel.

[17] Cauberghe, B. (2004). Applied Frequency-Domain System Identification in the Field of Experimental and Operational modal Analysis. Ph.D. thesis, Vrije University, Brussel.

[18] Peeters, B., ans P. Guillaume, T. D. T., and der Auweraer, V. (2006). In-flight modal analysis a comparison between sweep and turbulence excitation. In International Conference on Noise and Vibration Engineering. Leuven, Belgium.

[19] Troyer, T. D., Guillaume, P., and Runacres, M. C. (2012). Consistent multi-input modal parameter estimators in the frequency domain. Mechanical Systems and Signal Processing, 31, 130–142.

[20] Guillaume, P., Hermans, L., and der Auweraer, H. V. (1999). Maximum likelihood identification of modal parameters from operational data. In 17th International Modal Analysis Conference. Kissimmee, FL, USA.

[21] El-Kafafy, M., Guillaume, P., and Peeters, B. (2013). Modal parameter estimation by combining stochastic and deterministic frequency-domain approaches. Mechanical Systems and Signal Processing, 35, 52–68.

[22] Zeng, J. and Kukreja, S. L. (2013). Flutter prediction for flight/wind-tunnel flutter test under atmospheric turbulence excitation. Journal of Aircraft, 50(6), 1696–1709.

[23] Dimitriadis, G. and Cooper, J. E. (2001). Flutter prediction from flight flutter test data. Journal of Aircraft, 38(2), 355–367.

[24] Dimitriadis, G. and Cooper, J. E. (2006). Comment on flutter prediction from flight flutter test data. Journal of Aircraft, 43(3), 862–863.

[25] Lind, R. (2003). Flight-test evaluation of flutter prediction methods. Journal of Aircraft, 40(5), 964–970.

[26] Akaike, H. (1976). Canonical correlation analysis of time series and the use of an information criterion. In System Identification Advances and Case Studies, vol. 126 of Mathematics in Science and Engineering. Elsevier, pp. 27–96.

[27] Jury, I. and Pavlidis, T. (1963). Stability and aperiodicity constraints for system design. IEEE Transactionson Circuit Theory, 10(1), 137–141.

[28] Nahom, T., Kogan, T., Iovnovich, M., et al. (2016). Evaluation of an arma flutter boundary prediction method based on discrete-time structural responses to turbulence excitation in flight-tests. In 56th Israel Annual Conference on Aerospace Sciences. Tel-Aviv, Israel: Curran Associates, Inc.

[29] Balmes, E. (1996). Frequency domain identification of structural dynamics using the pole/residue parametrization. In International Modal Analysis Conference. pp. 194–200.

[30] Ljung, L. (1987). System Identification - Theory for the User. Englewood Cliffs, NJ: PrenticeHall.

[31] Welch, P. D. (1967). The use of fast fourier transform for the estimation of power spectra: A method based on time averaging over short modified periodograms. IEEE Trans. Audio Electracoust, AU-15, 70–73.

[32] El-Kafafy, M., Peeters, B., and ans P. Guillaume, T. D. T. (2013). Polymax plus estimator: Better estimation of the modal parameters and their confidence bounds. In International Conference on Noise and Vibration Engineering. Leuven, Belgium, pp. 2491–2505.

[33] Denegri, C. M. J. (2000). Limit cycle oscillation flight test results of a fighter with external stores. Journal of Aircraft, 37(5), 761–769.

[34] Denegri, C. M. J. and Dubben, J. A. (2003). In-flight wing deformation characteristic during limit cycle oscillations. In 44th AIAA/ASME/ASCE/AHS Structures, Structural Dynamics, and Materials Conference. Reston, VA: AIAA. AIAA-2003-1426.

COPYRIGHT STATEMENT